

# Strengthening of unreinforced masonry walls using ECC for impact/blast resistance

M. Maalej

*University of Sharjah, Sharjah, UAE*

V.W.J. Lin, M.P. Nguyen & S.T. Quek

*National University of Singapore, Singapore, Singapore*

**ABSTRACT:** This paper presents the results of quasi-static and low-velocity projectile impact tests on unreinforced masonry (URM) walls retrofitted with a cementitious-based material known as Engineered Cementitious Composite (ECC). A total of 18 masonry wall panels were tested to assess the extent to which ECC can enhance the impact/blast resistance of the strengthened masonry walls by subjecting these series of panels to three types of load patterns namely patch load, uniformly-distributed load and impact load. Test results reported in this paper demonstrate the efficiency of the ECC-strengthening system in improving the ductility of URM walls, increasing their ultimate load-carrying capacity, enhancing their resistance against multiple low-velocity impacts and preventing sudden and therefore catastrophic failure.

## 1 INTRODUCTION

In recent years increasing research efforts have been devoted towards the development of blast-resistant and blast-retrofit designs for building structures. For these structures, the first real defense against the effect of blast loading is the building exterior, which is commonly made of masonry. However, unreinforced masonry elements are primarily designed to withstand in-plane compression loads and wind loads with little consideration of the forces generated in accidental events such as earthquakes and blasts. In the occurrence of such events, the unreinforced masonry elements experience in-plane and out-of-plane horizontal loads which they are not designed for, and thus, they will not be able to withstand these additional forces.

Many methods were proposed to enhance this out-of-plane resistance, one of which was to use composites like FRP to strengthen the masonry wall. Studies have shown that FRP reinforcement could be easily attached onto the masonry wall, thereby increasing its out-of-plane resistance significantly (Ehsani 1995, Triantafillou 1998, Gilstrap and Dolan 1998). However, masonry walls strengthened with FRP usually failed with little or no ductility.

In general, the material performance requirements for impact/blast applications include (a) fracture energy to resist spalling, scabbing and punching, (b) strength to prevent penetration and perforation, (c) ductility for bending and residual strength and (d) damage tolerance to withstand multiple impacts (Maalej et al. 2005). In addition, material used for

retrofit applications should provide ease of installation and should also have minimum shrinkage deformation after installation.

In a study conducted by Zhang et al. (2004), a hybrid-fiber ECC using proper volume ratio of high and low modulus fibers was developed to better meet the functional requirement for impact- and blast-resistant structures. This hybrid-fiber ECC mix containing 0.5 % steel and 1.5 % Polyethylene (PE) fibers (by volume), has displayed an optimal balance between ultimate strength and strain capacity. Typical uniaxial compressive and tensile stress-strain curves of the hybrid-fiber ECC material are presented in Figures 1 and 2, respectively. Maalej et al. (2005) studied the high velocity impact resistance of this hybrid-fiber ECC experimentally, demonstrating its high energy absorbing capacity and its ability to resist multiple impacts with little spalling, fragment ejection and small crater size on the impact face. It was concluded from the above study that ECC is a good material for impact and blast-resistant design of building structures.

Apart from the mechanical properties of ECC mentioned thus-far, recent investigations conducted by Li and Li (2006) have also verified ECC as an outstanding repair material. It was proven in the study that the ductility of the repair material is essential for achieving durability in the repaired structure. In particular, ECC has a high tensile ductility that relaxes potential stress build-up in the repair layer under drying shrinkage conditions. This behavior was accomplished by the multiple micro-crack damage that minimizes the delamination at the

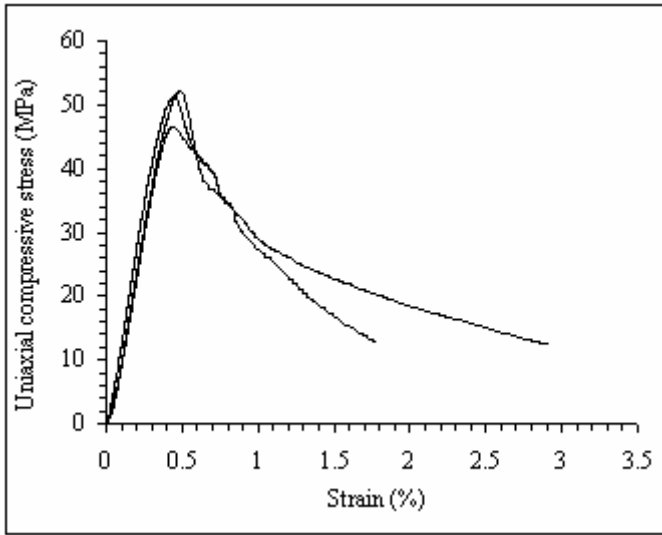


Figure 1. Typical hybrid-fiber ECC uniaxial compressive stress-strain curves.

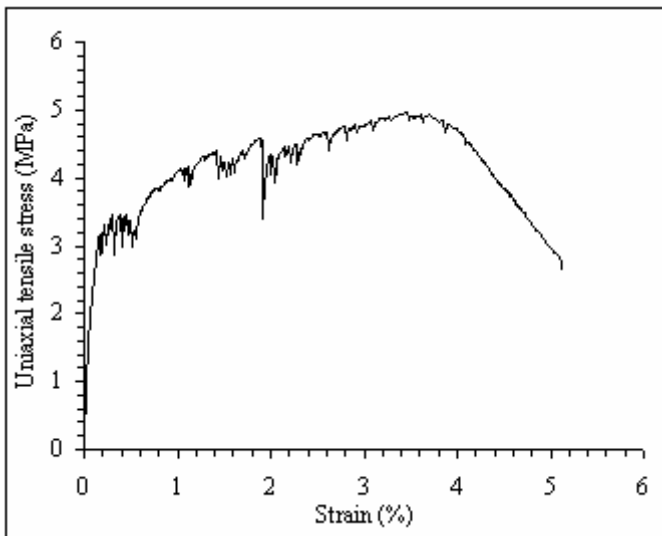


Figure 2. Typical hybrid-fiber ECC uniaxial tensile stress-strain curve.

interface. Therefore, ECC is expected to be a good material for strengthening unreinforced masonry structures against impact/blast loading.

The main objective of this research work is to investigate experimentally the behavior and effectiveness of ECC-strengthened masonry wall against impact/blast loading. As conducting a field test on strengthened walls under blast loading is difficult and expensive, three series of laboratory tests were carried out in this study to assess the extent to which ECC can enhance the impact/blast resistance of the strengthened masonry walls. These series of panels were subjected to three types of load patterns namely patch load, uniformly-distributed load and low-velocity projectile impact load.

## 2 EXPERIMENTAL PROGRAM

A total of 18 masonry wall panels were constructed and tested in the laboratory. Each wall panel meas-

ured 1000 x 1000 mm in plan and 100mm in thickness excluding the ECC layer. All walls were fabricated using solid clay bricks each having dimensions of 215 x 100 x 70 mm. The brick units were laid in running bond with mortar layers each approximately 10mm in thickness. ASTM Type 1 cement and plastering sand were used to prepare the mortar mix, for which the cement: sand proportions were 1:4 by volume. Five 100 x 100 x 70 mm bricks and fifteen 100mm mortar cubes were fabricated to determine its compressive strength.

The test specimens were grouped into three series, with Series I and II tests focusing on quasi-static loading, and Series III tests focusing on impact loading. Each series of test consisted of two unreinforced masonry walls (except Series III having one unreinforced masonry wall) to serve as control specimen and four strengthened masonry walls. Four strengthening configurations were studied, namely, (a) single-face of 34mm-thick ECC-strengthening layer (SE34), (b) double-face of 34mm-thick ECC-strengthening layer (DE34) each, (c) single-face of 34mm-thick ECC-strengthening layer with 8mm-diameter steel mesh (SD8) and (d) double-face of 34mm-thick ECC-strengthening layer with 8mm-diameter steel mesh (DD8) each. In Series I test, an additional reinforcing configuration, single-face of 20mm-thick ECC-strengthening layer (SE20) was included to investigate the effects of strengthening layer thickness variation. Each strengthened wall panel is identified using a combination of four to five characters. The first character, P (Patch), U (Uniformly distributed) or I (Impact) refers to the type of loading and the three to four characters that follow refer to the reinforcement configurations as describe above.

The ECC mix used was a hybrid-fiber mix containing 0.5 % steel fibers and 1.5 % high performance Polyethylene (PE) fibers. This was the mix proportion used in an earlier study on the performance of ECC under high velocity impact (Maalej et al. 2005); the only difference is that the diameter of the steel fiber used is 200  $\mu\text{m}$  instead of 160  $\mu\text{m}$ . The properties for the fibers used are shown in Table 1.

Table 1. Properties of fibers used.

Fiber Type	Length	Diameter	Elastic Mod.	Tensile Str.
	mm	$\mu\text{m}$	GPa	MPa
Steel	13	200	200	2500
Polyethylene	12	39	66	2610

### 2.1 Quasi-static load test set-up

The test set-ups for Series I and II are shown in Figures 3 and 4, respectively. The test wall was laid horizontal with the leveled face or the reinforced face downwards, and simply-supported along four

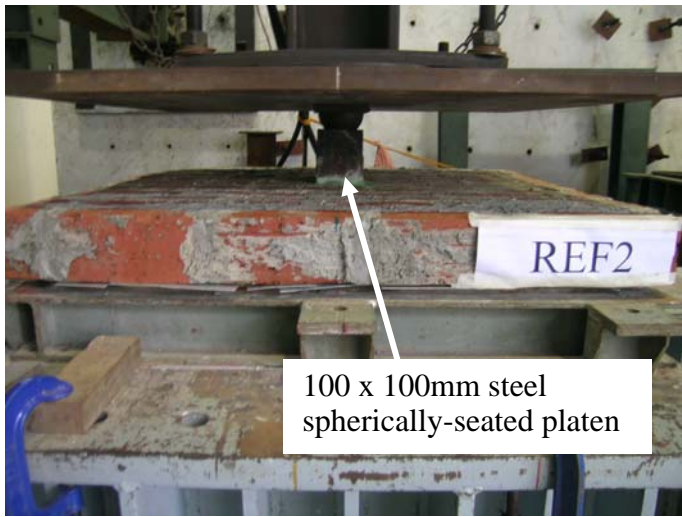


Figure 3. Quasi-static patch load test set-up.



Figure 5. Low-velocity projectile impact load test set-up.

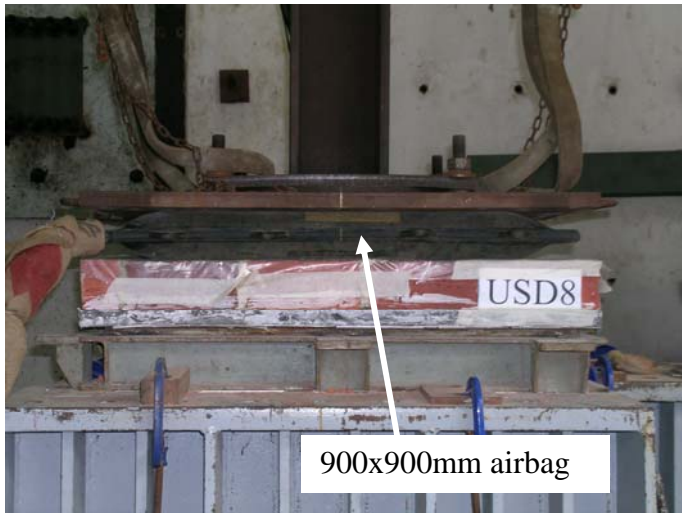


Figure 4. Quasi-static uniformly-distributed load test set-up.

sides on round steel bar supports without edge restraint. This means that the corners of the test wall were free to uplift. The effective span of the panel in both directions was 900mm.

The test set-ups for Series I and II were similar except for their loading areas. For Series I test, a patch load of 100 x 100 mm was applied at the center of the test specimen through a spherically-seated platen by means of a MTS hydraulic jack head and the load was applied using displacement control at a constant rate of 0.1 mm/min. For Series II test, a uniformly-distributed load of 780 x 780 mm was applied at the center of the test specimen using a Kevlar reinforced airbag of size 900 x 900 mm and the loading rate was controlled by the inflation of the airbag at an approximate rate of 1.5 kN/min.

## 2.2 Low-velocity projectile impact load test set-up

A drop weight impact facility similar to the one used by Ong et al. (1999) was adopted in this study (see Figure 5). This test facility consisted of a square steel frame welded on rigid columns that were bolted to the strong floor. Similarly, the specimen was laid horizontal with the leveled face or

reinforced face downwards, and simply-supported along four sides on round steel bars welded to a square frame. The effective span of the slab in both directions was 900mm. To prevent the specimen from bouncing under the impact, the test wall was clamped with a steel strip at the top face using G-clamps along the support line.

The impact was achieved by dropping a projectile of mass 51 kg from a height of 4 m. This test facility made use of a manually-operated winch system to raise the hammer to the desired height. The impact point was locked at the center of the test specimen using a vertical aluminum square guide. The hammer was then allowed to slide freely through the use of smooth rollers, greased to minimize friction effects. The average velocity of the projectile measured from the experiment was 8 m/s.

## 3 EXPERIMENTAL RESULTS

### 3.1 Quasi-static loading test results

The tests carried out for Series I walls subjected to 100 x 100 mm patch loading and Series II walls subjected to approximately 780 x 780 mm uniformly-distributed loading revealed five possible failure modes. They were: (a) tensile failure, (b) compression failure, (c) compression-induced buckling-bond failure (d) punching shear through the bricks and (e) shear de-bonding of the ECC-strengthening layer. These failure modes will be described and discussed in the analysis of results and discussion section.

The load-deflection responses of Series I and Series II test walls are shown in Figures 6 and 7, respectively. The applied load was recorded by the hydraulic actuator load cell, while the deflection of the specimen was measured at its center using a 100mm-range LVDT.

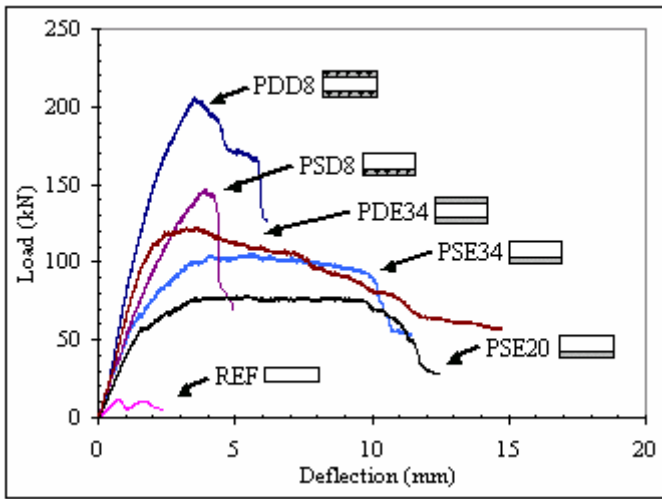


Figure 6. Load-deflection responses of wall components in Series I tests.

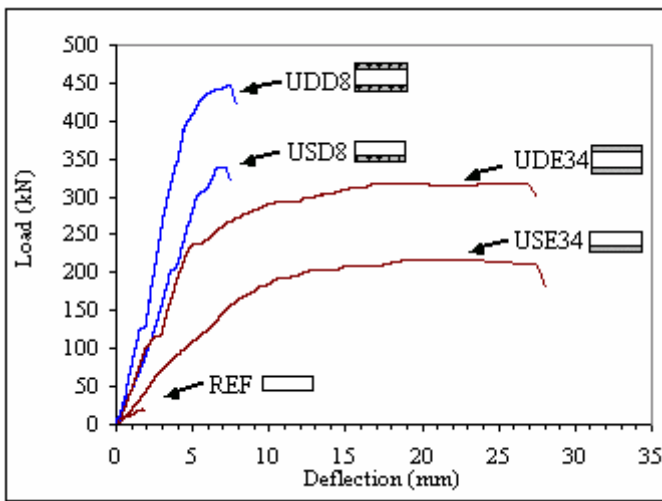


Figure 7. Load-deflection responses of wall components in Series II tests.

In general, the ECC-strengthening layer with or without steel mesh displayed very good stress distribution, having well-distributed cracks beneath the loading area stretching out towards the support in a radial pattern as shown in Figure 8. The only difference was that the cracks were less dense in the ECC-strengthening layer with the 8mm-diameter steel mesh indicating that the stresses were mostly distributed through the steel mesh. Lastly, it was interesting to note that as the steel mesh was pressing against the ECC layer, the shape of the steel mesh was visible from the crack patterns.

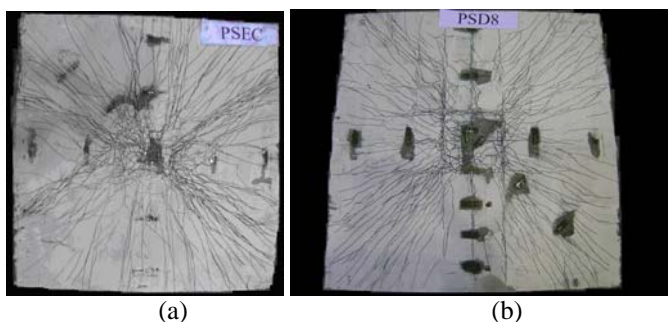


Figure 8. Typical cracking pattern of the ECC-strengthening layers (a) without steel mesh (b) with steel mesh

### 3.2 Low-velocity projectile impact loading test results

The importance of retrofitting an unreinforced masonry wall was demonstrated in this Series of tests when such wall exhibited sudden and therefore catastrophic failure upon its first impact loading. The unreinforced masonry wall was perforated by the projectile upon impact and shattered into a few pieces as shown in Figure 9. A large amount of fragment ejections were observed during the impact.



Figure 9. Failure of unreinforced masonry wall under impact loading.

All ECC-strengthened masonry walls were able to withstand multiple impacts before perforation—five for ISE34, nine for ISD8, nine for IDE34 and eighteen for IDD8. Furthermore, during the impact, no fragments ejection was observed at the surface with the ECC-strengthening layer. This observation demonstrated the ECC's ability to prevent fragmentations due to the impact, which may help reduce human injuries in the event of blast/explosion.

The impact load versus time graphs obtained from the first 3 impact loadings applied to Series III test walls are shown in Figures 10-13. In general, two peak loads can be identified from each of the impacts. The primary peak load occurs within 2 ms upon impact, corresponding to the instant when the projectile strikes the specimen accelerating it downwards, and the secondary peak load takes place when the accelerating specimen loses its kinetic energy and rebounds upward, increasing its contact pressure with the on-coming projectile.

On the whole, the duration of the impact (taken to be the time upon the impact until the load was smaller than 5 kN) ranges from 4.315 to 16.370 ms, depending on the interaction between the projectile and the specimen before the projectile rebounded.

## 4 ANALYSIS OF RESULTS AND DISCUSSION

### 4.1 Quasi-static loading tests

The results from the quasi-static tests have shown significant improvements in the ultimate load-carrying capacity and the ductility of the unreinforced masonry walls with the ECC-strengthening systems. The ultimate load-carrying capacity and deflection were used as comparison parameters to evaluate the performance of each reinforcing configuration. To be consistent in the comparison study, 90% post-ultimate load was selected as the cut-off point in the load-deflection curve, as most structures will still be able to function with 90% of the design strength. The results of Series I and II tests are summarised in Tables 2 and 3, respectively.

As mentioned earlier, five failure modes were observed from the experimental tests. Tensile failure was only observed in the unreinforced masonry walls in which the wall had little resistance against out-of-plane loading due to the low tensile strength of the masonry.

Compression failure was generally observed in the masonry walls that were singly-reinforced with ECC-strengthening layer without steel mesh (PSE20, PSE34 and USE34). In this reinforcing configuration, the tensile ECC layer had a significantly-high strain capacity, while the strain capacity at the compressive face remained unchanged. Therefore, when the wall experienced out-of-plane loading, the applied strain at the compressive face exceeded the strain capacity of the masonry and hence crushing of the masonry took place.

Compression-induced buckling-bond failure of the ECC layer was observed in the masonry walls that were doubly reinforced with ECC-strengthening system without steel mesh (PDE34 and UDE34). In the case of uniformly-distributed loading, however, the large loading area delayed this mode of failure, contributing to increased load-carrying capacity of the test wall (Fig. 7). In addition, comparing the load-deflection curves for specimens PSE34 and PDE34 on the one hand, and USE34 and UDE34 on the other hand, it seems that the large loading area in the latter case allowed Specimen UDE34 to preserve a high deflection capacity in comparison to Specimen PDE34.

Punching shear failure was observed in the masonry wall that was retrofitted using a single ECC-strengthening layer with steel mesh (PSD8). In this configuration, the additional 8mm-diameter steel mesh made the ECC-strengthening layer stiffer and harder to deform. In the case of patch loading, the inability of the reinforced wall to deform resulted in stress concentration near the loading area. Due to the brittle nature of the masonry material, at the moment when the load exceeded the punching shear capacity

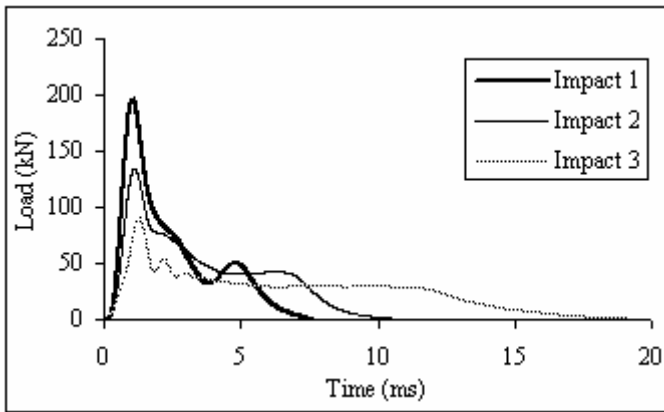


Figure 10. Load versus time graph for the first 3 impacts of ISE34.

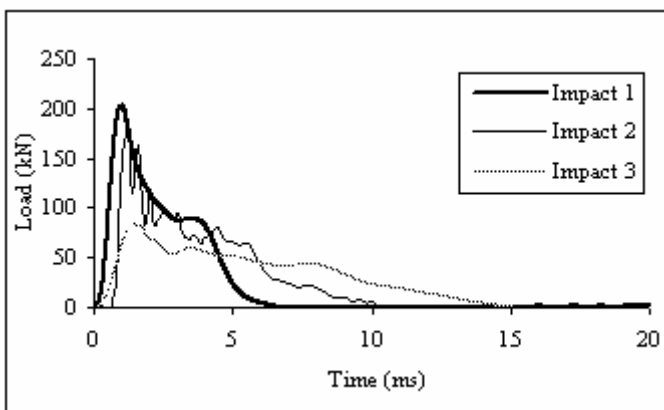


Figure 11. Load versus time graph for the first 3 impacts of ISD8.

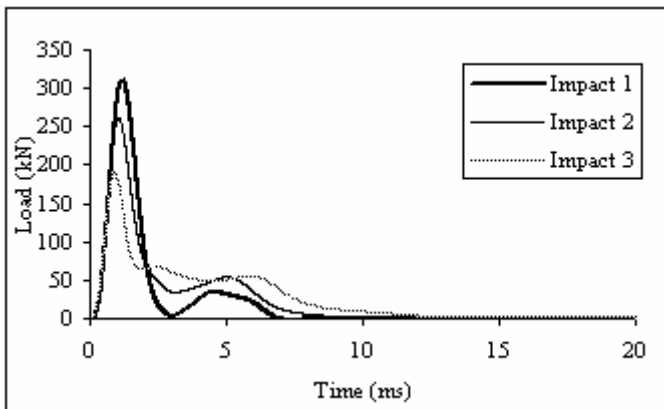


Figure 12. Load versus time graph for the first 3 impacts of IDE34.

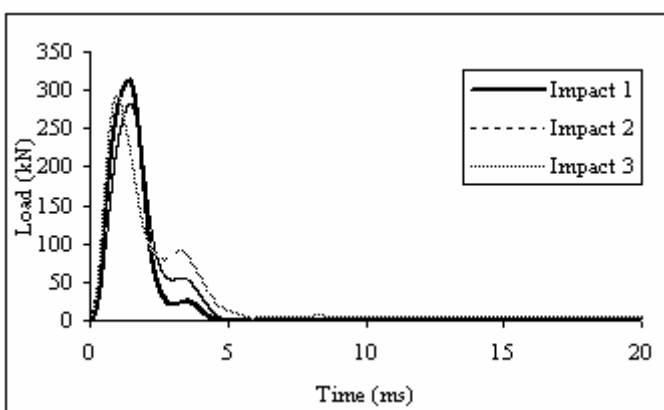


Figure 13. Load versus time graph for the first 3 impacts of IDD8.

Table 2. Summary of Series I tests results.

Specimen	Observed failure mode	Ultimate load-carrying capacity	Deflection	Energy absorption capacity
		kN	mm	Joules
REF	Tensile flexure	11.94	0.74	5.28
PSE20	Compression flexure	78.26	9.95	666.8
PSE34	Compression flexure	105.5	9.60	836.9
PDE34	Buckling-bonding	122.7	5.54	522.0
PSD8	Punching shear	146.9	4.35	398.7
PDD8	Shear de-bonding	206.6	4.53	621.9

Table 3. Summary of Series II tests results.

Specimen	Observed failure mode	Ultimate load-carrying capacity	Deflection	Energy absorption capacity
		kN	mm	Joules
REF	Tensile flexure	20.37	1.73	17.8
USE34	Compression flexure	217.9	27.5	3265
UDE34	Buckling-bonding	318.3	27.0	4978
USD8	Shear de-bonding	337.3	7.22	945
UDD8	Shear de-bonding	447.3	7.43	1456

of the masonry layer, punching failure took place without warning. The stresses were then transferred to the ECC-masonry interface causing it to de-bond.

Shear de-bonding failure was generally observed in the masonry walls that were doubly-reinforced with ECC-strengthening layer with steel mesh (PDD8, USD8 and UDD8). Here again, the additional 8mm-diameter steel mesh made the ECC-strengthening layer stiffer and harder to deform. In these cases, high shear stresses were built up at the ECC-masonry interface due to the unequal deformation of the ECC and masonry layer, leading to bond failure.

The test results shown in Tables 2 for Series I indicate that the ECC-strengthening system increased the failure loads and deflection capacities of the walls significantly by 6.5 to 17.3 times and 5.8 to 13.4 times, respectively, relative to those of the unreinforced masonry walls. Likewise, from Series II test results, the failure loads and deflection capacities were significantly increased by 10.7 to 22 times and 4.2 to 15.9 times, respectively, relative to those of the unreinforced masonry walls. The energy absorption for Series I and II masonry walls were significantly increased as well from 75 to 158 times and from 53 to 279 times, respectively, relative to those of the unreinforced masonry walls.

Lastly, it was observed from Series I and II tests that the ECC-strengthening systems incorporating the 8mm-diameter steel mesh possessed a higher ultimate load-carrying capacity with lesser ductility. This was because the additional steel mesh made the composite panel stiffer, thereby enhancing its load-carrying capacity but reducing its ability to deform. Hence, depending on the nature of the retrofitting application, different reinforcing configuration can be utilized.

#### 4.2 Thickness variation study of ECC-strengthening layer

Series I test results for the masonry walls incorporating single ECC-strengthening layers with 20mm- (PSE20) and 34mm- (PSE34) diameter steel mesh were used to study the effect of the thickness of the ECC layer on the load and deflection capacity. The load-deflection responses of the reinforced walls were similar as shown in Figure 6; the only difference was the ultimate load-carrying capacity. Despite being thicker by 70%, the ultimate load-carrying capacity of PSE34 was only 35% higher than that of PSE20. It was found from section analysis that the strain in the ECC-strengthening layers directly beneath the loading area of PSE20 and PSE34 was 3.54% and 2.43%, respectively (both below the tensile strain capacity of the ECC material). These observations suggest that in specimen PSE20 the ECC layer had a higher contribution to ultimate load-carrying capacity than in specimen PSE34.

#### 4.3 Low-velocity projectile impact loading tests

The behavior and physical damage suffered by the test walls under low-velocity projectile impact loading differed with different ECC-strengthening systems applied. As mentioned earlier, all ECC-strengthened masonry walls were able to withstand multiple impacts, hence, the degree of damage inflicted in the specimens under repeated impacts was of greater interest compared to the energy absorption capacity of the specimen under single impact. The damage level is evaluated and characterized based on the average crater diameter, indentation depth, crack propagation as well as fragmentation. The first two parameters were measured directly from the specimens after each test, while the rest were ob-

served qualitatively from high speed camera and digital camera recordings.

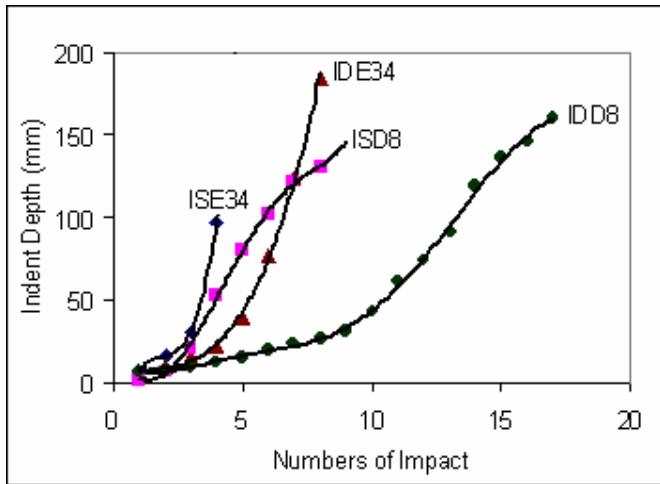


Figure 14. Plot of indent depth development.

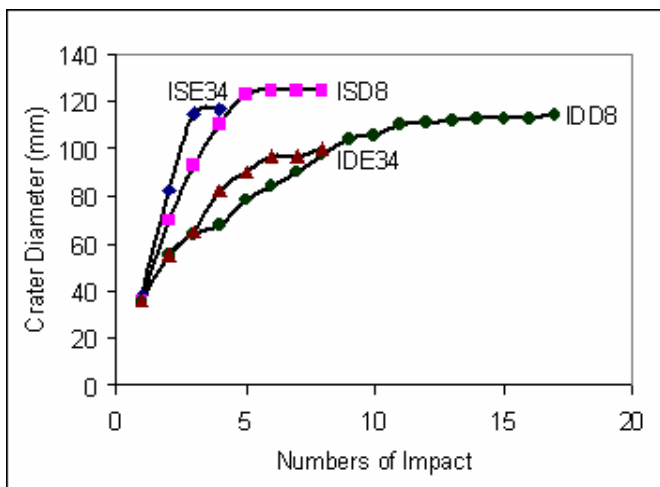


Figure 15. Plot of crater diameter development.

To evaluate the penetration resistance of each ECC-strengthening system, the indentation depths and crater diameters created on the impact face were plotted against the number of impacts as presented in Figures 14 and 15, respectively. From the two figures, it can be observed that the indentation depths as well as the crater sizes of the reinforced walls decreases with the addition of the 8mm-diameter steel mesh, for both singly and doubly-reinforced walls, at the same number of impacts. Double-faced reinforced masonry walls displayed higher penetration resistance with lesser indentation depth and smaller crater size compared with single-faced reinforced masonry walls. This is because the ductile ECC-strengthening layer at the impact face of the wall absorbed a significant part of the impact energy, thereby protecting the brittle masonry sandwich layer and resulting in a smaller degree of damage.

Figures 16-19 show the impact and distal faces of the specimens at perforation. All the ECC-strengthened masonry wall panels remained structurally intact and showed only localized damage af-

ter being perforated. In general, all reinforced walls had cracks on the distal side that propagated from the impact point towards the support edges. Under point-load impact, the panel tried to bend close to a conical shape with high hoop stress. The cementitious matrix of the ECC material being brittle then fractured but the cracks were arrested by the bridging action of the fibers, resulting in a well-distributed radial pattern. It was also observed that the ECC-strengthening layer without steel mesh had very densely distributed cracks, while the ECC-strengthening layer with steel mesh had cracks that were sparsely distributed, indicating that the stresses were largely distributed by the steel mesh rather than the ECC-strengthening layer.

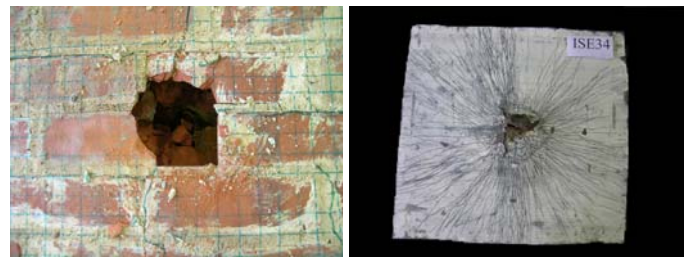


Figure 16. Impact and distal face of ISE34 after perforation.



Figure 17. Impact and distal face of ISD8 after perforation.

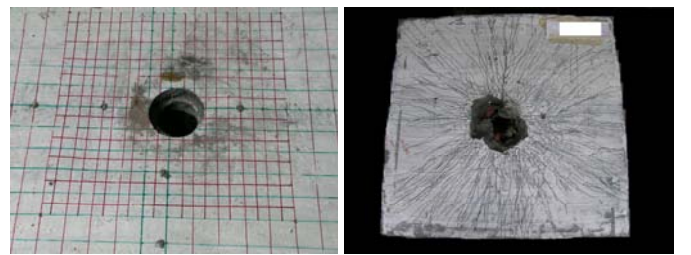


Figure 18. Impact and distal face of IDE34 after perforation.



Figure 19. Impact and distal face of IDD8 after perforation.

## 5 CONCLUSION

From the quasi-static loading tests, it was shown that The ECC-strengthening systems improved the out-of-plane resistance of the masonry walls significantly. In particular, the ultimate load-carrying ca-

capacity and maximum deflection of the masonry wall increased from 6.5 to 22 times and from 4.2 to 15.9 times for Series I and II tests, respectively. The steel mesh within the ECC-strengthening layer increased the ultimate load-carrying capacity of the reinforced wall by 40% to 68%, but reduced the deflection capacity of the specimen by 17% to 74%. The ability of ECC to strain-harden and develop multiple micro-cracks was also observed in this masonry retrofit application.

When subjected to low-velocity projectile impact, the ECC-strengthened masonry walls demonstrated an ability to resist multiple impact loadings, unlike URM which failed catastrophically when subjected to the first impact. The ECC-strengthening layers were also able to significantly reduce the fragmentations due to the impact, which will help to minimize human injuries due ejection of fragments in the event of blast/explosion.

In conclusion, it has been shown in this study that ECC-strengthening systems for URM are very effective in enhancing the wall impact resistance, and preventing sudden and catastrophic failure. These observations are positive indications that the ECC-strengthened masonry walls can also mitigate damages resulting from a blast/explosion event.

## REFERENCES

- Ehsani, M. R. 1995. Strengthening of Earthquake-Damage Masonry Structures with Composite Materials, in L. Taerwe ed. *Non-metallic (FRP) Reinforcement for Concrete Structures*. Spon, London. 680-687.
- Gilstrap, J. M. and Dolan, C. W. 1998. Out-of-Plane Bending of FRP-Reinforced Masonry Walls, *Composite Science and Technology*, v58. 1277-1284.
- Li, M., and Li, V. C. 2006. Behaviour of ECC/Concrete Layered Repair System under Drying Shrinkage Conditions. *Journal of Restoration of Buildings and Monuments*. v12 (2). 143-160.
- Maalej, M., Quek, S.T. and Zhang, J. 2005. Behavior of Hybrid-Fiber Engineered Cementitious Composites Subjected to Dynamic Tensile Loading and Projectile Impact. *Journal of Materials in Civil Engineering, ASCE*. v17 (2). 143-152.
- Ong, K. C. G., Basheerkhan, M. and Paramasivam, P. 1999. Resistance of Fiber Concrete Slabs to Low Velocity Projectile Impact, *Cement and Concrete Composite*. v21. 391-401.
- Triantafillou, T. C. 1998. Strengthening of Masonry Structures Using Epoxy-Bonded FRP Laminates. *Journal of Composites for Construction, ASCE*, v2 (2). 96-104.
- Zhang, J., Maalej, M. and Quek, S. T. 2004. Hybrid Fiber Engineered Cementitious Composites (ECC) for Impact and Blast-Resistant Structures, in *Proceedings of First International Conference on Innovative Materials and Technologies for Construction and Restoration-IMTCR04*. 6-9 June 2004, Lecce, Italy. 136-149.